ELSEVIER

Chemical Engineering Journal 136 (2008) 320–330

Chemical Engineering Journal

www.elsevier.com/locate/cej

Simulating the behavior of a wire mesh reactor for olive kernel fast pyrolysis

Th. Damartzis, G. Ioannidis, A. Zabaniotou *

Department of Chemical Engineering, Aristotle University of Thessaloniki, University Box 455, 24154 Thessaloniki, Greece

Received 14 December 2006; received in revised form 2 April 2007; accepted 3 April 2007

Abstract

The simulation of the behavior of a wire mesh reactor is presented in the following study making use of models extracted from the literature. Two different kinetic models are used, coupled with heat transfer model, mass conservation equations, continuity equations and momentum equations. The numerical method applied is finite difference for the momentum, mass conservation, heat transfer and continuity equations and Runge–Kutta fourth order for the chemical kinetic model equations. Simulations are carried out for spherical olive kernel particles with radius of 175 μm, reactor temperature 873 K and heating rates of 200 K/s. The simulation works satisfyingly under the hypothesis of ablative behavior and the results are in very good agreement with the experimental data regarding temperature, conversion histories and product distribution of olive kernel fast pyrolysis.

Keywords: Particle; Simulation; Fast pyrolysis; Wire mesh reactor; Diffusion; Product design

1. Introduction

There has been a growing interest in the renewable energy sources since the last decades, thus, the understanding of the physical and chemical mechanisms governing the phenomenon of pyrolysis must be well known in order to do the optimal design of chemical pyrolysis reactors.

Since the 1950s, the researchers' interest was directed towards energy production from coal. Therefore, physical and chemical mechanisms governing the phenomenon of thermo chemical conversion of coal is much studied. Biomass could be assumed to be converted in a similar way to coal, but in contrast with coal whose main component is lignin, biomass is consisted of cellulose and semi-cellulose, which makes the difference. In many cases the cellulose fraction is close to 80%. From the above, an assumption can be formed that the biomass pyrolysis could be simulated with cellulose pyrolysis, although experiments have shown that this is totally unacceptable due to the fact that there is an interaction between the biomass components during the pyrolysis procedure.

The precise mechanism of biomass pyrolysis is not known, because of the fact that many parallel and successive reactions are taking place, making the study of the phenomenon extremely hard. So, in order to study the phenomenon, researchers proposed simplified models with successive and parallel pseudo-first order reactions. These reactions describe, in a simple way, the transition from biomass to intermediate and final products.

Many models have been developed till recently for the transition of biomass to the final products. The Broido–Shafizadeh model is a well-known model, which was initially developed for cellulose pyrolysis but was reconstructed later in order to simulate the behavior of products which consist of cellulose, semi-cellulose and lignin. According to some researchers [1,2] the inorganic compounds of biomass can act as catalysts during pyrolysis. Considering this, one more reaction was later added at the initial Broido–Shafizadeh model through which biomass transits to an activated form. The Broido–Shafizadeh mechanism is shown in Fig. 1, where B refers to biomass, B* refers to activated biomass, T refers to tar, C refers to char and G refers to gas.

According to Koufopanos et al. [3], the concentration and fraction of the medium products can not be measured, so the activated biomass has only theoretical interest for the time being. The reaction of biomass to its activated form was questioned in the past from various researchers [4]. Specifically, it was proved

* Corresponding author. Tel.: +30 2310 996274; fax: +30 2310 996209.
E-mail address: sonia@cheng.auth.gr (A. Zabaniotou).

1385-8947/$ – see front matter © 2007 Published by Elsevier B.V.
doi:10.1016/j.cej.2007.04.010

Nomenclature

b	geometry factor (sphere = 3)
Bi_M	modified Biot number
C	concentration (kg/m^3)
C_p	specific heat capacity (J/mol K)
D	molar diffusion coefficient (m^2/s)
E	activation energy (J/mol)
h	convective heat transfer coefficient (W/m K)
k	thermal conductivity (W/m K)
k_i	rate constant (s^{-1})
k_m	mass transfer coefficient (m/s)
k_0	pre-exponential factor (s^{-1})
Le	Lewis number
m	reactor heating rate, K/s
n_i	reaction i order
P	absolute pressure (Pa)
Pr	Prandtl number
r	radial distance (m)
R	radius of sphere (m)
Re	Reynolds number
R_g	universal gas constant (J/mol)
Sh	Sherwood number
t	time (s)
T	temperature (K)
U	velocity (m/s)
W	molar weight (kg/mol)
W_i	% product yield of component i
x	dimensionless distance

Greek letters

α	thermal diffusivity (m^2/s)
γ	constant of Eq. (60)
ΔH	heat of reaction (J/kg)
ε	emissivity coefficient
ε''	porosity of particle
θ	dimensionless temperature
μ	viscosity (Pa s)
ν	kinematic viscosity (m/s)
ρ	density (kg/m^3)
σ	Stefan–Boltzmann coefficient (W/m^2 K^4)
τ	dimensionless time

Subscripts

0	initial values
B	biomass
C	char
f	final value
G	gases
G_1	(gases + tar)$_1$
G_2	(gases + tar)$_2$
T	tar

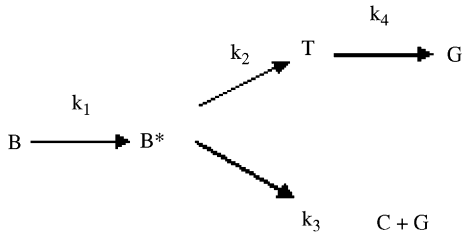

Fig. 1. The Broido–Shafizadeh mechanism.

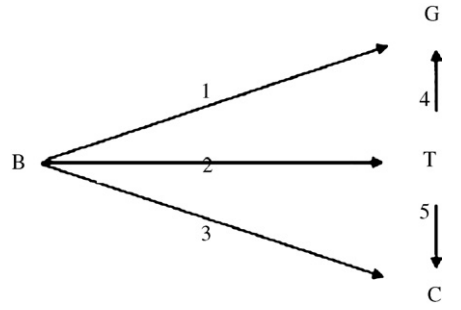

Fig. 2. Modified Broido–Shafizadeh mechanism.

that the simulation results were not in agreement with the laboratory results when the reaction was included. On the other hand, when the reaction was not included in the model, the results were quite promising.

The mechanism becomes more appealing when the reaction from tar to char is included. So, the final Broido–Shafizadeh mechanism is shown in Fig. 2. In recent studies, researchers [2,5–17] made the above models more accurate by incorporating momentum equations as well as mass and heat transfer equations inside and outside of the biomass particle. Heat is transferred via conduction inside the particle and via convection and radiation outside the particle. There is also mass and heat transfer inside the particle caused by the gases' diffusion. Finally, the gases velocity is being considered as a result of the pressure drop inside the particle, as well as the influence of the temperature and concentration to the physical properties of biomass. Koufopanos et al. [3] suggested the series of reactions shown in Fig. 3 is taking place.

The final Broido–Shafizadeh model was initially used from Jalan and Srivastana [8] coupled with an energy conservation equation in order to simulate wood pyrolysis, but Babu and Chaurasia [17] later improved the model adding a mass conservation equation for the gases and correlations for the gas pressure and velocity. The results of the improved model are pretty close to experimental results. Its only weak point is the fact that there is no distinction between the gases and tar, making the task to estimate the tar yield impossible. The model also

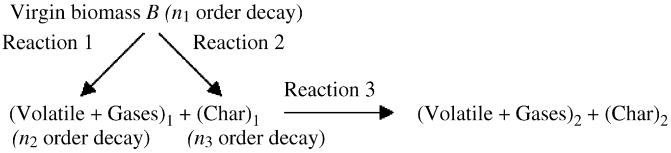

Fig. 3. Koufopanos mechanism.

assumes the diffusion of only the first reaction's gases is taking place, neglecting in this way the secondary gases' diffusion inside the particle.

The attempts to simulate pyrolysis with chemical kinetics of free radicals should also be mentioned as it is widely known that pyrolysis is taking place through complex mechanisms involving free radicals. But the difficulty of employing a model based on free radicals has forced the researchers to use simpler and more effective models. Bounaceur et al. [18] used a mechanism with radicals in order to simulate linear unsaturated hydrocarbon pyrolysis. In the past this has also been applied for the steam cracking of heavy petroleum residues [19].

In the present study two models have been studied. The above final Broido–Shafizadeh model is one of the two models examined and used in the simulations carried out. The second model used in this study is that proposed by Babu and Chaurasia [17], later improved by adding a mass conservation equation for the gases and correlations for the gas pressure and velocity. The ultimate purpose of this paper is to examine whether the experimental reactor can be simulated as an ablative or a fixed bed reactor.

2. Experimental

2.1. Materials

Pyrolysis of *olive kernel* samples was carried out in a laboratory captive sample reactor that could be identified as a wire mesh micro reactor (Fig. 4). The experiments were carried out at a temperature range of 573 K up to 873 K, heating rate 200 K/s for 1,5 s and gas/vapor residence times of approx. 0.5–1.0 s, at atmospheric pressure, under He. The technique enables the achievement of high heating rates as a prerequisite for short reaction periods. The results, which include the yields of the various pyrolysis products in relation to pyrolysis temperature as well as values for some kinetic constants, are presented in the literature [20] and are used in this study in order to obtain kinetic data for our simulations.

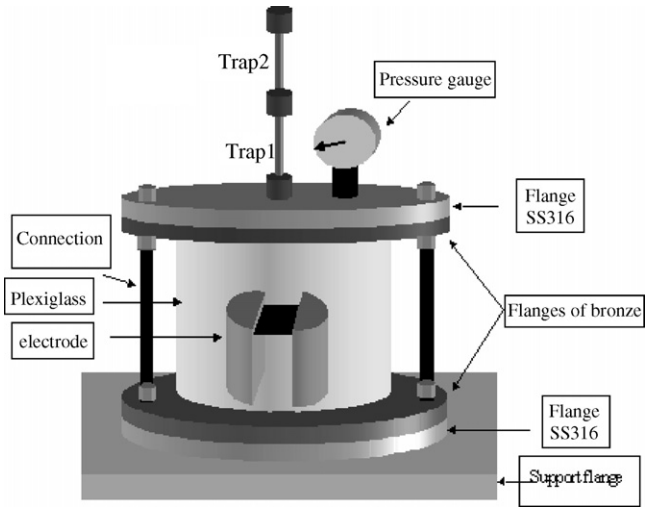

Fig. 4. The wire mesh reactor.

2.2. Reactor and experimental procedure

A captive sample reactor was used for the experiments. The procedure followed is presented in Fig. 5. The reactor is a cylindrical Plexiglass vessel with an inner diameter of 7 cm and is 12 cm high. The reactor vessel closes with two pairs of flanges (top and bottom). The upper pair of flanges is made of stainless steel SS316. Between the flanges, elastic o-ring is fitted, in order to achieve isolation. The stainless steel flange has a diameter of 12 cm and a thickness of 1 cm. In the centre there is a 0.3125 mm diameter hole serving for the gas exit, while on it are fitted a filter for tar collection and traps (T1, T2) for liquids collection. On the flange, a second similar hole serves for the fitting of a manometer, in order to measure the pressure in the reactor. Olive kernels were cut in pieces whose diameter was less than 500 mm. About 200 mg of the raw material is spread in a layer on a screen of stainless steel, which is inserted between the electrodes. Helium is passed through the reactor at the rate of 30 cm^3/min. The sample temperature is raised at the peak temperature. The reaction effluent includes fine charcoal, gas and volatile compounds. Their quenching occurs by natural cooling. The charcoal remains on the screen and is determined gravimetrically. Tar is defined as the material condensed within the reactor vessel, on the wall, flanges and on a paper filter at the exit of the reactor, at room temperature. Tar condensed inside the reactor is removed by washing with CH_2Cl_2 soaked filter paper and is measured gravimetrically. Hydrocarbons (in the vapor phase at room temperature) are collected in two lipophilic traps placed at the exit of the reactor and then measured gravimetrically. Gaseous products pass through two traps (T1 and T2), where the liquid HC are collected. Then, they pass through a water-cooling coil to be cooled to ambient temperature and then through a moisture collection trap, which is a cylindrical Plexiglass tube containing silica gel. Finally they reach the gas collection trap through the electrovalve TB. The volume of the removed water determines the gas volume. The gaseous products are selected in plastic sacs and they follow gas chromatography analysis.

The purpose of this study is to examine whether the experimental reactor which is a wire mesh or captive sample reactor could be simulated as an ablative or a fixed bed reactor, as they are the more relative configuration to a captive sample reactor and the most commonly used types of reactors. The functioning principle of an ablative reactor is the contact of the sample with a hot metal or the heating of the sample by means of radiation. There are two types of ablative reactors: contact ablative reactors and radiation ablative reactors.

In contact type reactors the sample is pressed on a hot surface resulting on the rapid heating of the external surface of the sample. The issue is that char formation on the surface is causing further resistance to heat transfer because char's thermal conductivity is less than that of biomass's and takes even lower values as temperature increases. Considering this, the design of ablative reactors is based on the removal of the external char layer. An example of this principle is the rotating disk ablative reactor. The ablative heat convection coefficient h_p, can be

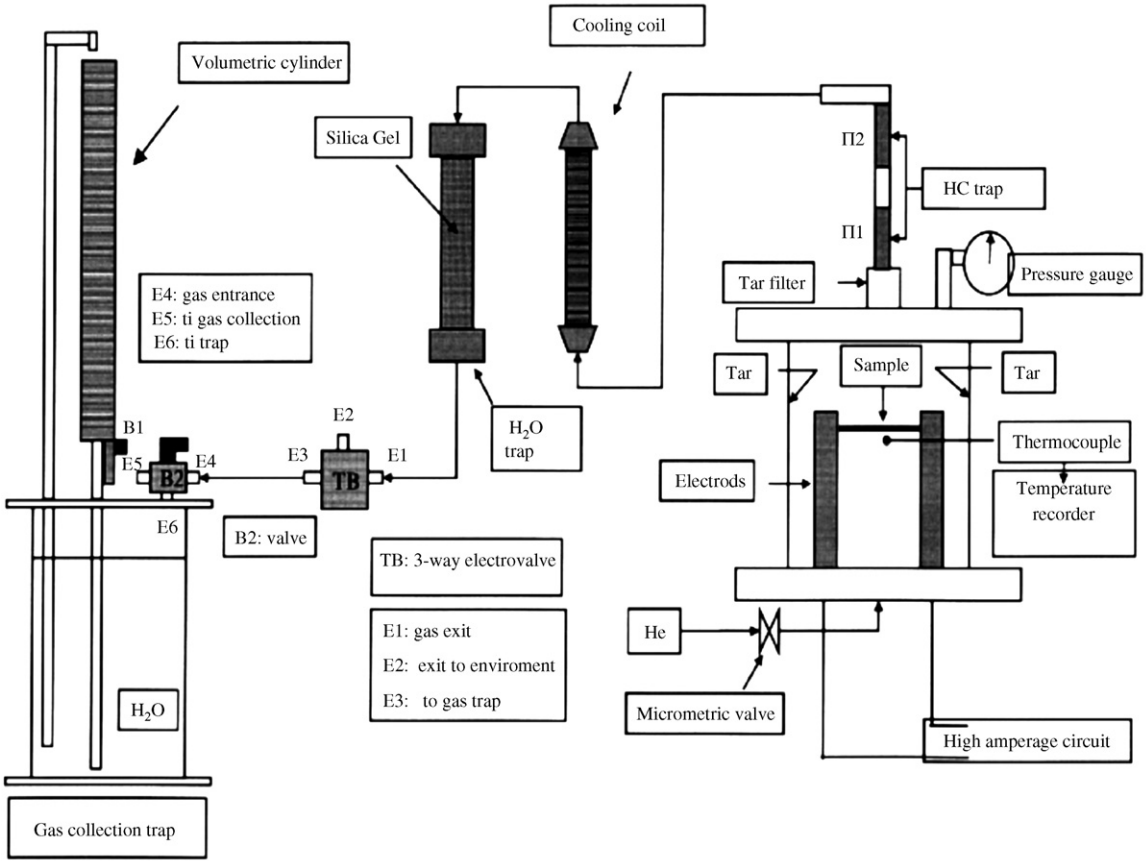

Fig. 5. Experimental procedure.

calculated from the following correlation taken from literature [21]:

$$h_p = 0.0017P \quad (1)$$

where P is pressure measured in Pa.

3. Formulation of mathematical models

In this study, two kinetic models are used in addition to mass, heat and momentum transport equations in order to simulate the behavior of the experimental wire mesh reactor. The behavior of the reactor is then compared to the behavior of the fixed bed and ablative reactor. The mechanism suggested by Koufopanos et al., which has been used by Babu and Chaurasia is presented in Table 1 with the chemical kinetic, the heat, mass and momentum transfer equations (Model I). The initial and boundary conditions are also being displayed in Table 1.

Shrinkage of biomass particles has been studied by Colomba Di Blasi [22] and Babu and Chaurasia [23]. According to Colomba Di Blasi, shrinkage is negligible for particles with a radius smaller than 2 mm. On the other hand, it is pretty important for large particles as the volume loss can be up to 70% of the initial volume. As a result, biomass and tar physical properties become a function of time. The latter has also been studied in the past by Colomba Di Blasi [24]. In this study, particle shrinkage was considered negligible as the size of the particles is too small (175 μm) for shrinkage to take effect.

The assumptions being made for the development of the model are the following:

- The particles are of spherical shape.
- Heat, mass and momentum transfer are taking place only in the radial dimension.
- Heat transfer inside the particle is taking place via conduction and convection and outside the particle via convection, conduction and radiation (conduction and radiation are appointed to the hot metal surrounding the particles and the reactor wall).
- The gases formed inside the particle pores are ideal.
- The reactor temperature is 873 K.
- Local phase equilibrium between solid and gas phases.
- Tar condensation inside the particle pores is negligible.
- Negligible particle shrinkage.
- Negligible heat resistance due to the external char and tar layer formed by the contact with the hot mesh.

In Table 2, the dimensionless forms of Eqs. (62)–(69) are being displayed. The dimensionless groups used, are shown in Table 3.

The second model which was used in the present study is the final Broido–Shafizadeh mechanism (Model II) coupled with mass, heat and momentum equations in a pretty similar way

Table 1
Model I equations

$$\frac{dC_B}{dt} = -(k_1 + k_2)C_B{}^{n_1} \tag{2}$$

$$\frac{dC_{C_1}}{dt} = k_2 C_B^{n_1} - k_3 C_{G_1}^{n_2} C_{C_1}^{n_3} \tag{3}$$

$$\frac{dC_{G_2}}{dt} = k_3 C_{G_1}^{n_2} C_{C_1}^{n_3} \tag{4}$$

$$\frac{dC_{C_2}}{dt} = k_3 C_{G_1}^{n_2} C_{C_1}^{n_3} \tag{5}$$

Mass, heat and momentum transfer equations are displayed below

$$\frac{\partial(C_{G_1}\varepsilon'')}{\partial t} + \frac{\partial(C_{G_1}U)}{\partial r} = D_{G_1}\left(\frac{b-1}{r}\frac{\partial C_{G_1}}{\partial r} + \frac{\partial^2 C_{G_1}}{\partial r^2}\right) + k_1 C_B^{n_1} - \varepsilon'' k_3 C_{G_1}^{n_2} C_{C_1}^{n_3} \tag{6}$$

$$\frac{\partial(\rho C_p T)}{\partial t} = k\left(\frac{b-1}{r}\frac{\partial T}{\partial r} + \frac{\partial^2 T}{\partial r^2}\right) - \left(D_{G_1}\frac{\partial C_{G_1}}{\partial r}\right) C_{P_{G_1}}\frac{\partial T}{\partial r} + (-\Delta H)\left(-\frac{\partial \rho}{\partial t}\right) \tag{7}$$

$$\frac{\partial \rho}{\partial t} = \frac{\partial C_B}{\partial t} + \frac{\partial C_{C_1}}{\partial t} + \frac{\partial C_{C_2}}{\partial t} = -k_1 C_B^{n_1} \tag{8}$$

$$\frac{\partial U}{\partial t} + U\frac{\partial U}{\partial r} = -\frac{1}{\rho}\frac{\partial P}{\partial r} + v\left(\frac{b-1}{r}\frac{\partial U}{\partial r} + \frac{\partial^2 U}{\partial r^2}\right) \tag{9}$$

With initial conditions

$t=0\ C_B = C_{B_0}, C_{G_1} = C_{G_2} = C_{C_1} = C_{C_2} = 0, T(r,0) = T_0, U(r,0) = U_0$

And boundary conditions

(10)–(11)$r = 0, t > 0 \quad \frac{\partial C_{G_1}}{\partial r} = 0, \quad \frac{\partial T}{\partial r} = 0$

$$r = R, t > 0 \quad D_{G_1}\left(\frac{\partial C_{G_1}}{\partial r}\right) = k_m(C_{G_{1,0}} - C_{G_1}) \tag{12}$$

$$r = R, t > 0 \quad k\frac{\partial T}{\partial r} = (h + h_p)(T_f - T) + \sigma\varepsilon(T_f^4 - T^4) \tag{13}$$

Table 2
Dimensionless forms of Model I equations

$$\frac{d\bar{C}_B}{dt} = -(k_1 + k_2)\bar{C}_B^{n_1} \tag{14}$$

$$\frac{d\bar{C}_{C_1}}{dt} = k_2 \bar{C}_B^{n_1} - k_3 \bar{C}_{G_1}^{n_2} \bar{C}_{C_1}^{n_3} \tag{15}$$

$$\frac{d\bar{C}_{G_2}}{dt} = k_3 \bar{C}_{G_1}^{n_2} \bar{C}_{C_1}^{n_3} \tag{16}$$

$$\frac{d\bar{C}_{C_2}}{dt} = k_3 \bar{C}_{G_1}^{n_2} \bar{C}_{C_1}^{n_3} \tag{17}$$

$$\varepsilon''\frac{\partial(\bar{C}_{G_1})}{\partial \tau} + \frac{UR}{\alpha}\frac{\partial \bar{C}_{G_1}}{\partial x} = \frac{\bar{D}_{G_1}}{Le}\left(\frac{b-1}{x}\frac{\partial \bar{C}_{G_1}}{\partial x} + \frac{\partial^2 \bar{C}_{G_1}}{\partial x^2}\right) + \frac{k_1 \bar{C}_B^{n_1}}{a} - \frac{\varepsilon'' k_3 \bar{C}_{G_1}^{n_2} \bar{C}_{C_1}^{n_3}}{a} \tag{18}$$

$$\rho C_p \frac{\partial \theta}{\partial \tau} = \frac{b-1}{x}\frac{\partial \theta}{\partial x} + \frac{\partial^2 \theta}{\partial x^2} + \frac{\bar{D}_{G_1}}{Le}\frac{\partial \bar{C}_{G_1}}{\partial x}\bar{C}_{P_G}\bar{C}_{B_0}\frac{\partial \theta}{\partial x} + \frac{Q''R^2 k_1}{a} \tag{19}$$

$$\frac{\partial \rho}{\partial t} = \frac{\partial \bar{C}_B}{\partial t} + \frac{\partial \bar{C}_{C_1}}{\partial t} + \frac{\partial \bar{C}_{C_2}}{\partial t} = -k_1 \bar{C}_B^{n_1} \tag{20}$$

$$\frac{\partial U}{\partial \tau} + U\frac{R}{a}\frac{\partial U}{\partial x} = -\frac{R}{a\rho}\frac{\partial P}{\partial x} + \frac{v}{a}\left(\frac{b-1}{x}\frac{\partial U}{\partial x} + \frac{\partial^2 U}{\partial x^2}\right) \tag{21}$$

Initial conditions

$\tau = 0 \quad \bar{C}_B = \bar{C}_{B_0}, \bar{C}_{G_1} = \bar{C}_{G_2} = \bar{C}_{C_1} = \bar{C}_{C_2} = 0, \theta(x,0) = 1, U(x,0) = U_0$

Boundary conditions

(22)–(23)$x = 0, t > 0 \quad \frac{\partial \bar{C}_{G_1}}{\partial x} = 0, \quad \frac{\partial \theta}{\partial x} = 0$

$$x = 1, t > 0 \quad \bar{D}_{G_1}\left(\frac{\partial \bar{C}_{G_1}}{\partial x}\right) = Sh(\bar{C}_{G_{1,0}} - \bar{C}_{G_1}) \tag{24}$$

$$x = 1, t > 0 \quad \frac{\partial \theta}{\partial x} = -\theta Bi_M \tag{25}$$

The gases' pressure inside the porous particle is given by

$$p = \frac{C_{G_1} R_g T}{W_g} \tag{26}$$

$$\text{the dimensionless form is : } \frac{\partial p}{\partial x} = \frac{R_g C_{B_0}}{W_g}\left[\left(\frac{T_f}{T_0 - T_f} + \theta\right)\frac{\partial \bar{C}_{G_1}}{\partial x} + \bar{C}_{G_1}\frac{\partial \theta}{\partial x}\right] \tag{27}$$

Table 3
Dimensionless groups

$a = k/\rho C_p$

$x = r/R$

$\tau = at/R^2$

$\theta = (T - T_f)/(T_0 - T_f)$

$Bi_M = (R/k)[(h + h_p) + \varepsilon\sigma(T^3 + T^2T_f + T_f^2T + T_f^3]$

$Q = (-\Delta H + C_pT)/\rho C_p(T_0 - T_f)$

$Q'' = QC_B^{n_1}$

$Le = k/(\rho_0 C_{P_{G_{1,0}}} D_{G_{1,0}})$

$Sh = (k_{m_{G_1}} R)/D_{G_{1,0}}$

$\bar{C}_B = C_B/C_{B_0}$

$\bar{C}_{B_0} = C_{B_0}/\rho_0$

$\bar{C}_{G_1} = C_{G_1}/C_{B_0}$

$\bar{C}_{G_{1,0}} = C_{G_{1,0}}/C_{B_0}$

$\bar{C}_{C_1} = C_{C_1}/C_{B_0}$

$\bar{C}_{G_2} = C_{G_2}/C_{B_0}$

$\bar{C}_{C_2} = C_{C_2}/C_{B_0}$

$\bar{C}_T = C_T/C_{B_0}$

$\bar{C}_{TB} = \bar{C}_T/\bar{C}_B$

$\bar{C}_{P_{G_1}} = C_{P_{G_1}}/C_{P_{G_{1,0}}}$

$\bar{D}_{G_1} = D_{G_1}/D_{G_{1,0}}$

with the previous model. The assumptions for the development of this model are almost the same. The main difference with the previous model is that gas and tar are considered to be two different phases, so there are separate mass conservation equations for tar and gas. The equations of this model are shown in Table 4. The dimensionless forms of the equations of Model II are shown in Table 5.

4. Numerical solution and simulation

The procedure followed for the two models is the same. The mass, heat and momentum transfer equations are solved numerically by finite difference method and the chemical kinetic equations are solved simultaneously with the fourth order Runge–Kutta method.

The constant b in the differential equations has been set equal to 3 which appoints to spherical coordinates. The time and space intervals chosen for the solution were separated in ten equal intervals, respectively. The two groups of equations (transfer and kinetic equations), are considered to be independent. The transfer equations are solved in each time interval and the profiles resulting from each interval's right end are used in order to provide temperature and concentration values for the set of kinetic equations. These values that are used to solve the kinetic equations with the Runge–Kutta fourth order method are the mean values of the temperature and concentration profiles arising from the solution of the transfer equations. The major impact of this method is that the reactions are assumed to be taking place isothermally in each time interval. Each time

Table 4
Model II equations

$$\frac{dC_B}{dt} = -(k_1 + k_2 + k_3)C_B \quad (28)$$

$$\frac{dC_C}{dt} = k_2C_B + \varepsilon'' k_5 C_T \quad (29)$$

$$\frac{\partial(C_G\varepsilon'')}{\partial t} + \frac{\partial(C_GU)}{\partial r} = D_G\left(\frac{b-1}{r}\frac{\partial C_G}{\partial r} + \frac{\partial^2 C_G}{\partial r^2}\right) + k_1C_B + \varepsilon'' k_4 C_T \quad (30)$$

$$\frac{\partial(C_T\varepsilon'')}{\partial t} + \frac{\partial(C_TU)}{\partial r} = D_G\left(\frac{b-1}{r}\frac{\partial C_T}{\partial r} + \frac{\partial^2 C_T}{\partial r^2}\right) + k_3C_B - \varepsilon''(k_4 + k_5)C_T \quad (31)$$

$$\frac{\partial(\rho C_pT)}{\partial t} = k\left(\frac{b-1}{r}\frac{\partial T}{\partial r} + \frac{\partial^2 T}{\partial r^2}\right) - \left(D_G\frac{\partial(C_G + C_T)}{\partial r}\right)C_{P_G}\frac{\partial T}{\partial r} + (-\Delta H)\left(-\frac{\partial \rho}{\partial t}\right) \quad (32)$$

$$\frac{\partial \rho}{\partial t} = \frac{\partial C_B}{\partial t} + \frac{\partial C_C}{\partial t} = -(k_1 + k_3)C_B + \varepsilon'' k_4 C_T \quad (33)$$

$$\frac{\partial U}{\partial t} + U\frac{\partial U}{\partial r} = -\frac{1}{\rho}\frac{\partial P}{\partial r} + v\left(\frac{b-1}{r}\frac{\partial U}{\partial r} + \frac{\partial^2 U}{\partial r^2}\right) \quad (34)$$

With initial conditions

$t = 0\ C_B = C_{B_0},\ C_G = C_C = C_T = 0,\ T(r, 0) = T_0,\ U(r, 0) = U_0$

And boundary conditions

(35)–(37) $r = 0, t > 0 \quad \frac{\partial C_G}{\partial r} = 0,\ \frac{\partial C_T}{\partial r} = 0,\ \frac{\partial T}{\partial r} = 0$

$$r = R, t > 0 \quad D_G\left(\frac{\partial C_G}{\partial r}\right) = k_m(C_{G_0} - C_G) \quad (38)$$

$$r = R, t > 0 \quad D_G\left(\frac{\partial C_T}{\partial r}\right) = k_m(C_{T_0} - C_T) \quad (39)$$

$$r = R, t > 0 \quad k\frac{\partial T}{\partial r} = (h + h_p)(T_f - T) + \sigma\varepsilon(T_f^4 - T^4) \quad (40)$$

Table 5
Dimensionless forms of Model II equations

$$\frac{d\bar{C}_B}{dt} = -(k_1 + k_2 + k_3)\bar{C}_B \quad (41)$$

$$\frac{d\bar{C}_C}{dt} = k_2\bar{C}_B + \varepsilon'' k_5 \bar{C}_T \quad (42)$$

$$\varepsilon''\frac{\partial \bar{C}_G}{\partial \tau} + \frac{UR}{a}\frac{\partial \bar{C}_G}{\partial x} = \frac{\bar{D}_G}{Le}\left(\frac{b-1}{x}\frac{\partial \bar{C}_G}{\partial x} + \frac{\partial^2 \bar{C}_G}{\partial x^2}\right) + \frac{k_1\bar{C}_B + \varepsilon'' k_4 \bar{C}_T}{a} \quad (43)$$

$$\varepsilon''\frac{\partial \bar{C}_T}{\partial \tau} + \frac{UR}{a}\frac{\partial \bar{C}_T}{\partial x} = \frac{\bar{D}_G}{Le}\left(\frac{b-1}{x}\frac{\partial \bar{C}_T}{\partial x} + \frac{\partial^2 \bar{C}_T}{\partial x^2}\right) + \frac{k_3\bar{C}_B - \varepsilon''(k_4 + k_5)\bar{C}_T}{a} \quad (44)$$

$$\frac{\partial \theta}{\partial \tau} = \left(\frac{b-1}{x}\frac{\partial T}{\partial x} + \frac{\partial^2 T}{\partial x^2}\right) + \left(\frac{\bar{D}_G}{Le}\frac{\partial(\bar{C}_G + \bar{C}_T)}{\partial x}\right)\bar{C}_{P_G}\bar{C}_{B_0}\frac{\partial \theta}{\partial x} + \frac{Q''R^2}{a}\left[(k_1 + k_3) - \varepsilon'' k_4 \bar{C}_{TB}\right] \quad (45)$$

$$\frac{\partial \rho}{\partial t} = \frac{\partial \bar{C}_B}{\partial t} + \frac{\partial \bar{C}_C}{\partial t} = -(k_1 + k_3)\bar{C}_B + \varepsilon'' k_4 \bar{C}_T \quad (46)$$

$$\frac{\partial U}{\partial \tau} + \frac{UR}{a}\frac{\partial U}{\partial x} = -\frac{R}{a\rho}\frac{\partial P}{\partial x} + \frac{v}{a}\left(\frac{b-1}{x}\frac{\partial U}{\partial x} + \frac{\partial^2 U}{\partial x^2}\right) \quad (47)$$

Initial conditions

$\tau = 0 \quad \bar{C}_B = \bar{C}_{B_0}, \bar{C}_G = \bar{C}_C = \bar{C}_T = 0, \theta(x,0) = 1, U(x,0) = U_0$

Boundary conditions

(48)–(50) $x = 0, t > 0 \quad \frac{\partial \bar{C}_G}{\partial x} = 0, \frac{\partial \bar{C}_T}{\partial x} = 0, \frac{\partial \theta}{\partial x} = 0$

$$x = 1, t > 0 \quad \bar{D}_G\left(\frac{\partial \bar{C}_G}{\partial x}\right) = Sh(\bar{C}_{G_0} - \bar{C}_G) \quad (51)$$

$$x = 1, t > 0 \quad \bar{D}_G\left(\frac{\partial \bar{C}_T}{\partial x}\right) = Sh(\bar{C}_{T_0} - \bar{C}_T) \quad (52)$$

$$x = 1, t > 0 \quad \frac{\partial \theta}{\partial x} = -\theta Bi_M \quad (53)$$

Pressure drop will be estimated by the equation

$$\frac{\partial p}{\partial x} = \frac{R_g C_{B_0}}{W_g}\left[\left(\frac{T_f}{T_0 - T_f} + \theta\right)\frac{\partial(\bar{C}_G + \bar{C}_T)}{\partial x} + (\bar{C}_G + \bar{C}_T)\frac{\partial \theta}{\partial x}\right] \quad (54)$$

interval though, is small enough so that the deviation from the real non-isothermal progressing of the reactions is negligible for this paper. Thus it is considered that each reaction is simulated with a series of successive isothermal reactions of the same form.

The correlations and values of physical properties are shown in Tables 6 and 7, respectively.

The rate constants of the reactions are considered to be Arrhenius type and they are all experimentally measured except from the rate constants of the secondary reactions which are found in the literature. The values of the rate constants are shown in Table 8.

5. Results and discussion

5.1. Kinetic constant calculation

Kinetic constants have been calculated by using experimental data from the wire mesh reactor (Fig. 6). As stated in the literature [20], the decomposition of biomass can be described by the following equation:

$$\frac{dW_i}{dt} = k_{0i}\, e^{-E_i/R_c T}(W_i^* - W_i) \quad (61)$$

Table 6
Correlations of properties used in the numerical solution of the models [23]

Correlations of physical properties	Equations	
Specific heat capacity of biomass	$C_p = 112 + 4.85(T - 273)$	(55)
Thermal conductivity of biomass	$k = 0.13 + 0.0003(T - 273)$	(56)
Specific heat capacity of gas/tar	$\bar{C}_p = 1 + P_1(\theta - 1); \quad P_1 = 0.001$	(57)
Diffusion coefficient of gas/tar	$\bar{D}_G = (\theta)^{P_1}\exp[P_2(1 - \bar{C}_B)]; \quad P_1 = 1.5, P_2 = 1$	(58)
Sherwood number	$Sh = P_1(\theta)^{P_2}; \quad P_1 = 50000, P_2 = 1$	(59)
Porosity	$\varepsilon'' = \varepsilon_0'' + \gamma(1 - \bar{C}_B)$	(60)

Table 7
Values of properties used in the numerical solution of the model

Physical Property	Value
Convective heat transfer coefficient	$h = 8.4\ \mathrm{W/m^2\ K}$, $T < 673\ \mathrm{K}$ [23] $h = 20\ \mathrm{W/m^2\ K}$, $T > 673\ \mathrm{K}$ [23]
Heat of reaction	$\Delta H = -255{,}000\ \mathrm{J/kg}$ [9]
Initial density	$\rho = 650\ \mathrm{kg/m^3}$ [23]
Thermal diffusivity of biomass	$\alpha = 1.79 \times 10^{-7}\ \mathrm{m^2/s}$ [23]
Initial particle porosity	$\varepsilon_0'' = 0.5$ [23]
γ constant (Eq. (60))	$\gamma = 0.3$ [23]
Viscosity of gas/tar	$\mu = 5 \times 10^{-5}\ \mathrm{Pa\,s}$ [23]
Molar weight of gas/tar	$W_g = 2.8 \times 10^{-3}\ \mathrm{kg/mol}$ [23]
Stefan–Boltzmann constant	$\sigma = 5.67 \times 10^{-8}\ \mathrm{W/m^2\ K^4}$
Emissivity coefficient	$\varepsilon = 0.95$ [23]
Universal constant of ideal gases	$R = 8.314\ \mathrm{J/mol\ K}$
Reaction order 1 (Model I)	$n_1 = 1$
Reaction order 2 (Model I)	$n_2 = 1$
Reaction order 3 (Model I)	$n_3 = 1.5$ [23]
Reaction order (Model II)	$n = 1$
Particle radius range	$R = 0.000175$–$0.001\ \mathrm{m}$
Initial temperature	$T_0 = 573\ \mathrm{K}$
Final temperature range	$T_f = 773$–$973\ \mathrm{K}$
Initial concentration of biomass	$C_{B0} = 650\ \mathrm{kg/m^3}$
Initial concentration of gases (Model I)	$C_{G_{10}} = C_{G_{20}} = 0$
Initial concentration of char (Model I)	$C_{C_{10}} = C_{C_{20}} = 0$
Initial concentration of gases (Model II)	$C_{G_{10}} = 0$
Initial concentration of char (Model II)	$C_{C_{10}} = 0$
Initial concentration of tar (Model II)	$C_{T_0} = 0$

Table 8
Rate constants of reactions

Model	Reaction	Rate constant	$k_0\ (\mathrm{s^{-1}})$	E (kJ/mol)
I	1	k_1	1.6×10^4	46.65
	2	k_2	8.05×10^2	32.1
	3	k_3	5.7×10^5 [23]	81 [23]
II	1	k_1	9.8×10^5	61
	2	k_2	3.7×10^2	29.27
	3	k_3	8.05×10^2	32.1
	4	k_4	8.6×10^4 [26]	87.8 [26]
	5	k_5	7.7×10^4 [26]	87.8 [26]

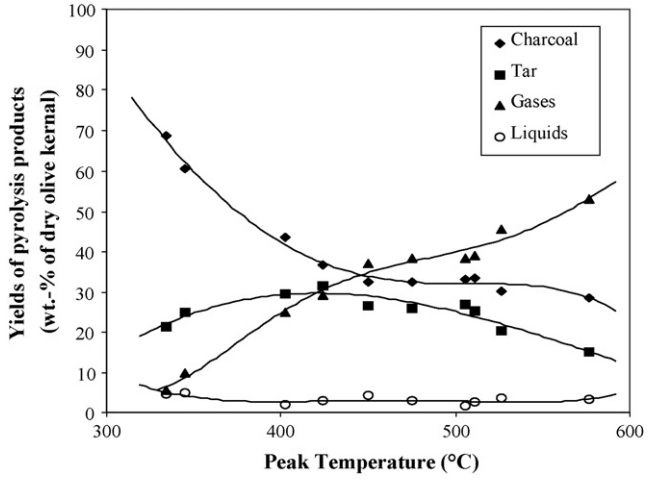

Fig. 6. Product distribution from experimental study.

where W_i is the % yield of the pyrolysis product i at time t and W_i* is the maximum attainable yield of i at infinite time.

Since the change of W_i with time is unknown, the first part of Eq. (61) can be written as

$$\frac{\mathrm{d}W_i}{\mathrm{d}t} = \frac{\mathrm{d}W_i}{\mathrm{d}T}\frac{\mathrm{d}T}{\mathrm{d}t} = \frac{\mathrm{d}W_i}{\mathrm{d}T}m \tag{62}$$

where m is the heating rate of the reactor (K/s).

The combination of Eqs. (61) and (62) gives:

$$\frac{\mathrm{d}W_i}{W_i^* - W_i} = \frac{k_{0i}}{m}\,\mathrm{e}^{-E_i/R_cT}\,\mathrm{d}T \tag{63}$$

Integration of Eq. (63) with the help of Cauchy's formula and the assumption that $2RT/E_i \ll 1$ gives:

$$\ln\left(\frac{1}{T^2}\ln\frac{W_i^*}{W_i^* - W_i}\right) = \ln\left(\frac{k_{0i}R_c}{mE_i}\right) - \left(\frac{E_i}{R}\right)\frac{1}{T} \tag{64}$$

which is a linear first order equation, resembling the basic form $y = \alpha x + b$. By plotting $\ln(1/T^2 \ln(W_i^*/W_i^* - W_i))$ as a function of $1/T$ and determining the values for α and b, one can calculate E_i and k_{0i} from the following equations:

$$a = \frac{-E}{R} \tag{65}$$

$$b = \ln\left(\frac{k_{0i}R_c}{mE_i}\right) \tag{66}$$

The values of W_i and W_i* were taken from Fig. 6 for the sum of gas and tar and E_1 and k_1 for Model I were calculated. Their values are: $E_1 = 46{,}650\ \mathrm{J/mol}$ and $k_{01} = 1.6 \times 10^4\ \mathrm{s^{-1}}$.

Using E_1, k_{01} and the experimental results, values of k_2 were calculated for various temperatures with the help of the following analogy, taken from literature [25]:

$$\frac{k_1 + k_2}{k_2} = \frac{W_G + W_C}{W_C} \tag{67}$$

where W_G is the % yield of gas and tar at a given temperature and W_C is the % yield of char at the same temperature.

Values of $\ln k_2$ were then plotted against $1/T$. The plot is a straight line with the basic form: $y = \alpha x + b$. E_2 and k_{02} were calculated by the use of the following equations:

$$a = \frac{-E_2}{R} \tag{68}$$

$$b = \ln k_{02} \tag{69}$$

The calculated values of E_2 and k_{02} are: $E_2 = 32{,}100\ \mathrm{J/mol}$ and $k_{02} = 805\ \mathrm{s^{-1}}$. The kinetic constants for Model II were calculated in the same way.

5.2. Comparison of the models' results with experimental data

The simulation results concerning the two models are in a very good agreement with the experimental results issued from the captive sample reactor. Gas and tar yield conversion as a function of temperature is shown in Fig. 7. The radius of the spherical particle is 175 μm and the final reactor temperature

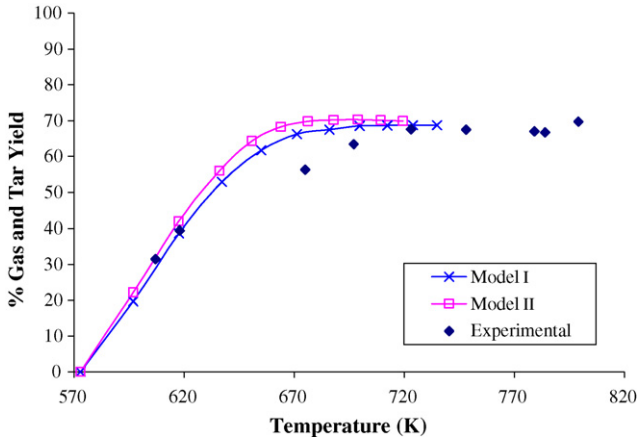

Fig. 7. Yield of gas and tar as a function of temperature.

is 873 K. Model I seems to be in a slightly better agreement than Model II. Nevertheless, the final yield arising from the simulation of both models is exactly the same. In correspondence to Fig. 7, the conversion of char as a function of temperature is shown in Fig. 8. The ablative convection heat transfer coefficient from Eq. (61) is utilized for these simulations.

5.3. The ablative effect

The wire mesh reactor, in which the experiments were conducted, should have a mixed behavior in-between the ablative reactor and the fixed bed reactor. Fixed bed reactors do not include the ablative heat convection coefficient as it is described in Eq. (61). The wire mesh reactor operates at atmospheric pressure, and no pressure is applied to the mesh capturing the sample. So, the ablative convection heat transfer coefficient for pressure valued equal to 1 bar or 100,000 Pa, is found to be (from Eq. (61)) 170 W/m^2 K. It is obvious that the ablative coefficient is far superior to the convection heat transfer coefficient considered in the fixed bed's function. As a result the heat flux is greater, leading to faster temperature increase of the particles and decreasing in this way the pyrolysis time. This phenomenon is shown in Figs. 9 and 10 for Models I and II, respectively.

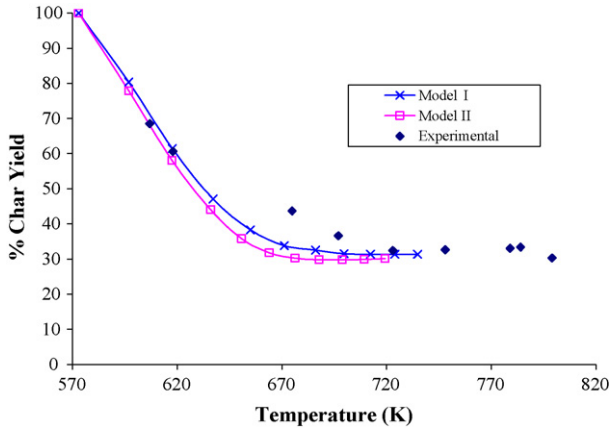

Fig. 8. Char yield as a function of temperature.

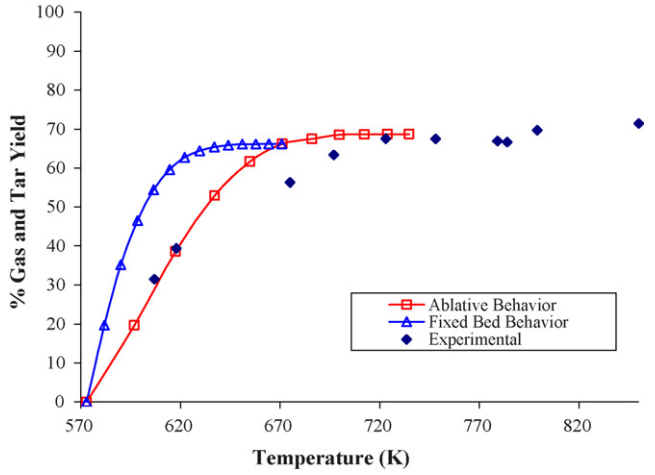

Fig. 9. The ablative effect in Model I.

From the above, it is derived that the wire mesh reactor can be simulated better as an ablative reactor.

When taking into consideration the ablative effect, the final yield of gas and tar appears to be slightly higher (2%) in Model I than it is in Model II. If the values of the rate constants of reactions in Table 8 are observed (for Model I), it is profound that k_1 will increase much more than k_2 with temperature increase. As a result the difference between k_1 and k_2 increases as the temperature rises, leading to higher yields of gas and tar. On the other hand, the final yield observed in Model II is the same for fixed bed and ablative behavior. This phenomenon is taking place because of the secondary reactions and more specifically because of the 5th reaction which describes the tar transition to char. As a result, tar yield is decreased, leading to the decrease of total gas and tar yield.

In Tables 9 and 10, the results of the simulations for ablative and fixed bed behavior are shown for Models I and II, respectively. It is observed that the time needed for pyrolysis to take place is less in ablative behavior than in fixed bed behavior, which is appointed to the higher value of the ablative coefficient h_p.

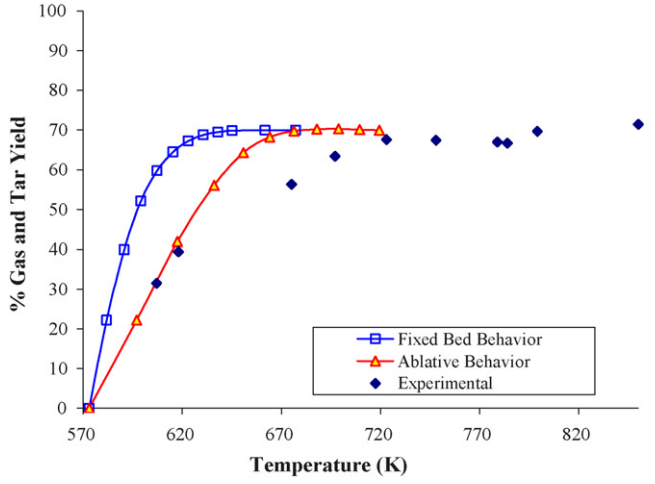

Fig. 10. The ablative effect in Model II.

Table 9
Results of the simulation for ablative and fixed bed behavior for Model I

Ablative behavior		Fixed bed behavior	
Time (s)	Remaining biomass (%)	Time (s)	Remaining biomass (%)
0	100	0	100
0.018	69.07	0.018	69.07
0.036	41.15	0.036	44.24
0.054	20.93	0.054	26.72
0.072	8.86	0.072	15.2
0.09	3.07	0.09	8.11
0.108	0.86	0.108	4.04
0.126	0.19	0.126	1.87
0.144	0.03	0.144	0.77
0.162	4×10^{-3}	0.162	0.3
0.18	0	0.18	0.11
		0.198	0.04
		0.216	0.01
		0.234	0

Table 10
Results of the simulation for ablative and fixed bed behavior for Model II

Ablative behavior		Fixed bed behavior	
Time (s)	Remaining biomass (%)	Time (s)	Remaining biomass (%)
0	100	0	100
0.018	69.37	0.018	69.37
0.036	39.26	0.036	42.52
0.054	19.69	0.054	25.43
0.072	8.41	0.072	14.61
0.09	3.09	0.09	7.93
0.108	0.97	0.108	4.05
0.126	0.26	0.126	1.94
0.144	0.06	0.144	0.87
0.162	1.1×10^{-3}	0.162	0.36
0.18	0	0.198	0.04
		0.234	0

5.4. Product distribution over time

In Figs. 11 and 12, yields of gas, tar, char and biomass as a function of time are shown for Models I and II, respectively. It is observed that pyrolysis has been completed in less than

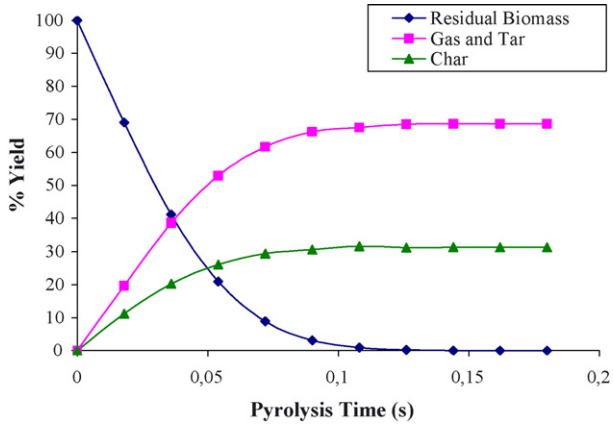

Fig. 11. Yield of biomass, gas, tar and char as a function of pyrolysis time for Model I.

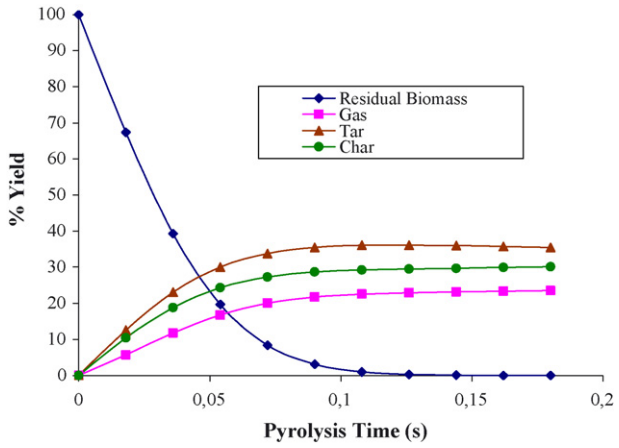

Fig. 12. Yield of biomass, gas, tar and char as a function of pyrolysis time for Model II.

0.2 s. This fact provides information about the residence time demanded for the completion of fast pyrolysis.

6. Conclusions

In the present study two models were used in order to simulate the behavior of an experimental wire mesh reactor/captive sample reactor for the fast pyrolysis of olive kernel. The models are consisted of two different pyrolysis mechanisms coupled with heat, mass and momentum transfer equations for spherical biomass particles. The results arising from our simulations showed that:

- Both models are in very good agreement with the experimental data. Model I showed a slightly better agreement than Model II.
- The laboratory wire mesh reactor is simulating better with an ablative reactor rather than a fixed bed one.

References

[1] O. Boutin, M. Ferrer, J. Lede, Flash pyrolysis of cellulose pellets submitted to a concentrated radiation: experiments and modelling, Chem. Eng. Sci. 57 (2002) 15–25.
[2] Colomba Di Blasi, Comparison of semi-global mechanisms for primary pyrolysis of lignocellulosic fuels, J. Anal. Appl. Pyrol. 47 (1) (1998) 43–64.
[3] C.A. Koufopanos, N. Papayannakos, G. Maschio, A. Lucchesi, Modelling of the pyrolysis of biomass particles—studies on kinetics, thermal and heat transfer effects, Can. J. Chem. Eng. 69 (1991) 907–915.
[4] V. Gabor, Michael Jerry Antal Jr., J. Emma, S. Piroska, Kinetic modelling of biomass pyrolysis, J. Anal. Appl. Pyrol. 42 (1) (1997) 73–87.
[5] Colomba Di Blasi, Heat transfer mechanisms and multi-step kinetics in the ablative pyrolysis of cellulose, Chem. Eng. Sci. 51 (1996) 2211–2220.
[6] Colomba Di Blasi, Modelling the fast pyrolysis of cellulosic particles in fluid-bed reactors, Chem. Eng. Sci. 55 (2000) 5999–6013.
[7] D.L. Pyle, C.A. Zaror, Heat transfer and kinetics in the low temperature pyrolysis of solids, Chem. Eng. Sci. 39 (1984) 147–158.
[8] R.K. Jalan, V.K. Srivastava, Studies on pyrolysis of a single biomass cylindrical pellet—kinetic and heat transfer effects, Energy Convers. Manage. 40 (1999) 467–494.
[9] Colomba Di Blasi, Physico-chemical processes occurring inside a degrading two-dimensional anisotropic porous medium, Int. J. Heat Mass Transfer 41 (1998) 4139–4150.

[10] B.V. Babu, A.S. Chaurasia, Modelling for pyrolysis os a solid particle: kinetics and heat transfer effects, Energy Convers. Manage. 44 (2003) 2251–2275.
[11] Sung-Chul Yi, R.H. Mohammad, Product distribution from the pyrolysis modelling of tobacco particles, J. Anal. Appl. Pyrol. 66 (9) (2003) 217–234.
[12] L.T. Fan, L.S. Fan, K. Miyanami, T.Y. Chen, W.P. Walawender, Mathematical model for pyrolysis of a solid particle—effects of Lewis number, Can. J. Chem. Eng. 55 (1977) 47–53.
[13] K. Miyanami, L.S. Fan, W.P. Walawander, Mathematical model for pyrolysis of a solid particle—effects of heat of reaction, Can. J. Chem. Eng. 55 (1977) 317–325.
[14] H.C. Kung, A mathematical model of wood pyrolysis, Combust. Flame 18 (1972) 185–195.
[15] E.J. Kansa, H.E. Perlee, R.F. Chaiken, Mathematical model of wood pyrolysis—Including internal forced convection, Combust. Flame 29 (1977) 311–324.
[16] C.H. Bamford, J. Crank, D.H. Mala, Combustion of wood, in: Proceedings Cambridge Philosophical Society, vol. 42, 1946, pp. 166–182.
[17] B.V. Babu, A.S. Chaurasia, Pyrolysis of biomass: improved models for simultaneous kinetics and transport of heat, mass and momentum, Energy Convers. Manage. 45 (2004) 53–72.
[18] R. Bounaceur, V. Warth, P.M. Marquaire, G. Scacchi, F. Domine, D. Desort, Modelling of hydrocarbons pyrolysis at low temperature. Automatic generation of free radicals mechanisms, J. Anal. Appl. Pyrol. 64 (2002) 103–122.
[19] Dominique Depeyre, Chantal Flicoteaux, Ferechthe Arbabzadeh, Anastasia Zambaniotou, Modelling of thermal steam cracking of an atmospheric gas–oil, Ind. End Eng. Chem. Res. 28 (1989) 967–976.
[20] A.A. Zabaniotou, G. Kalogiannis, E. Kappas, A.J. Karabelas, Olive residues (cuttings and kernels) rapid pyrolysis product yields and kinetics, Biomass Bioenergy 18 (2000) 411–420.
[21] Colomba Di Blassi, Heat transfer mechanisms and multi-step kinetics in the ablative pyrolysis of cellulose, Chem. Eng. Sci. 51 (1996) 2211–2220.
[22] Colomba Di Blasi, Heat, momentum and mass transport through a shrinking biomass particle exposed to thermal radiation, Chem. Eng. Sci. 51 (1996) 1121–1132.
[23] B.V. Babu, A.S. Chaurasia, Heat transfer and kinetics in the pyrolysis of a shrinking biomass particle, Chem. Eng. Sci. 59 (2004) 1999–2012.
[24] Colomba Di Blasi, Influences of physical properties on biomass devolatilization characteristics, Fuel 76 (10) (1997) 957–964.
[25] B.M. Wagenaar, W. Prins, W.P.M. Van Swaaij, Flash pyrolysis kinetics of pine wood, Fuel Process. Technol. 36 (1993) 291–298.
[26] A.M.C. Janse, R.W.J. Westerhout, W. Prins, Modelling of flash pyrolysis of a single wood particle, Chem. Eng. Process. 39 (2000) 239–252.